QUARTERLY JOURNAL OF THE ROYAL METEOROLOGICAL SOCIETY
Q. J. R. Meteorol. Soc. **133**: 181–196 (2007)
Published online in Wiley InterScience
(www.interscience.wiley.com) DOI: 10.1002/qj.8

Effects of data selection and error specification on the assimilation of AIRS data†

J. Joiner,[1]* E. Brin,[2] R. Treadon,[3] J. Derber,[3] P. Van Delst,[3] A. Da Silva,[4] J. Le Marshall,[3] P. Poli,[5] R. Atlas,[6] D. Bungato[2] and C. Cruz[7]

[1] *NASA Goddard Space Flight Center Laboratory for Atmospheres, USA*
[2] *Science Applications International Corporation, USA*
[3] *Joint Center for Satellite Data Assimilation, USA*
[4] *NASA Goddard Space Flight Center Global Modeling and Assimilation Office, USA*
[5] *Centre National de Recherches Météorologiques, Météo France, Toulouse, France*
[6] *NOAA Atlantic Oceanographic and Meteorological Laboratory, USA*
[7] *NGITI, USA*

ABSTRACT: The Atmospheric InfraRed Sounder (AIRS), flying aboard NASA's Aqua satellite with the Advanced Microwave Sounding Unit-A (AMSU-A) and four other instruments, has been providing data for use in numerical weather prediction and data assimilation systems for over three years. The full AIRS data set is currently not transmitted in near-real-time to the prediction/assimilation centres. Instead, data sets with reduced spatial and spectral information are produced and made available within three hours of the observation time. In this paper, we evaluate the use of different channel selections and error specifications. We achieve significant positive impact from the Aqua AIRS/AMSU-A combination during our experimental time period of January 2003. The best results are obtained using a set of 156 channels that do not include any in the H_2O band between 1080 and 2100 cm^{-1}. The H_2O band channels have a large influence on both temperature and humidity analyses. If observation and background errors are not properly specified, the partitioning of temperature and humidity information from these channels will not be correct, and this can lead to a degradation in forecast skill. Therefore, we suggest that it is important to focus on background error specification in order to maximize the impact from AIRS and similar instruments. In addition, we find that changing the specified channel errors has a significant effect on the amount of data that enters the analysis as a result of quality control thresholds that are related to the errors. However, moderate changes to the channel errors do not significantly impact forecast skill with the 156 channel set. We also examine the effects of different types of spatial data reduction on assimilated data sets and NWP forecast skill. Whether we pick the centre or the warmest AIRS pixel in a 3×3 array affects the amount of data ingested by the analysis but does not have a statistically significant impact on the forecast skill. Published in 2007 by John Wiley & Sons, Ltd.

KEY WORDS forecast; numerical; weather; climate; radiances; satellite

Received 5 May 2006; Revised 20 September 2006; Accepted 18 October 2006

1. Introduction

The Atmospheric Infra-Red Sounder (AIRS) (Aumann *et al.*, 2003) is the first of several advanced high-spectral-resolution nadir-viewing passive infrared sounders to be used for climate applications and operational numerical weather prediction (NWP). AIRS is a grating spectrometer that has been flying on the National Aeronautics and Space Administration's (NASA) Earth Observing System (EOS) polar-orbiting Aqua platform since May 2002 along with the Advanced Microwave Sounding Unit - A (AMSU-A) and four other instruments. Over the next few years, additional kilochannel interferometers will fly in Low Earth Orbit. These include the Infrared Atmospheric Sounding Interferometer (IASI) on the EUMETSAT MetOp platform and the Cross-Track Infrared Sounder (CrIS) on the National Polar-orbiting Operational Environmental Satellite System (NPOESS) series of satellites as well as the NASA/National Oceanic and Atmospheric Administration (NOAA)/(US) Department of Defense (DoD) NPOESS Preparatory Project (NPP).

In order to facilitate near-real-time (NRT) transmission of the voluminous AIRS data, the complete AIRS data set must be reduced. There are several possible methods of data reduction. These include channel and/or pixel subsetting and methods such as principle component analysis that represent only the most important modes of the spectral information content. Before launch, the NOAA National Environmental Satellite Data and Information Service (NESDIS) set up a special processing system to provide several different data sets to the NWP and data assimilation community (Goldberg *et al.*, 2003).

* Correspondence to: J. Joiner, NASA Goddard Space Flight Center, Code 613.3, Greenbelt, MD, 20771, USA.
E-mail: Joanna.Joiner@nasa.gov

Shortly after launch, the NWP and data assimilation centres began to receive subsetted AIRS NRT data. Positive impact on NWP skill has been demonstrated (e.g. Le Marshall *et al*., 2006; McNally *et al*., 2006; Chahine *et al*., 2006) and AIRS data assimilation is now (or will soon be) operational at several NWP centres.

This paper examines data assimilation strategies for AIRS observations and their impact on NWP. Specifically, we investigate the impact of using several channel subsets, assigning different spectrally-dependent errors, and applying two types of spatial data reduction. Section 2 describes the AIRS instrument and data preprocessing in detail. The data assimilation system (DAS) and experimental setup are discussed in sections 3 and 4, respectively. Results from several assimilation experiments are presented in section 5. A discussion focused on the effects of H_2O band channels follows in section 6. Conclusions and suggestions for further research are provided in section 7.

2. AIRS instrument and data pre-processing

AIRS is a cooled array grating spectrometer with 2378 channels covering the spectral range 650–2674 cm^{-1} with a resolving power ($\nu/\Delta\nu$) of 1200. The instrument scans cross track over a swath width of 1650 km. The footprint diameter is approximately 13.5 km at the nadir from the nominal orbital height of 705 km which corresponds to a field-of-view size of 1.1°. The reduced data sets used here contain a 281 channel subset of the 2378 available AIRS channels. These channels are listed in Table 1. European NWP centres receive a slightly different dataset with 324 channels. The extra channels are primarily located in the CO_2 and H_2O absorption bands.

Figure 1 shows the normalized weighting functions for three representative AIRS channels centred at 704.4, 1524.4, and 1045.3 cm^{-1}. These channels are affected primarily by CO_2, H_2O, and O_3 absorption, respectively. The weighting functions were computed using a midlatitude profile. The weighting function widths shown in Figure 1b are defined as the range for which the function is at or greater than 90% of its peak value for a given peak.

These weighting functions illustrate a few points that are important to consider for assimilation. Firstly, H_2O-absorbing channels can have sharper weighting functions than those in the CO_2 bands. Secondly, channels may be sensitive to more than one absorber or analysis variable. For example, the 1045.3 cm^{-1} channel has two peaks, one due to O_3 absorption in the stratosphere and one due primarily to H_2O absorption in the lower troposphere. H_2O-absorbing channels are also quite sensitive to the vertical temperature structure. These two facts highlight the difficulties associated with using the data properly. The information in the brightness temperatures must be correctly partitioned between the different analysis variables. In addition, the channels with the highest vertical resolution (e.g. in the H_2O band) may be more complicated to interpret than other channels (e.g. those in the CO_2 bands).

Figure 2 shows a simulated AIRS brightness temperature spectrum with the 281 channel subset highlighted. It can be seen in the long-wave CO_2 absorption band (e.g. between ~720–740 cm^{-1}) and in the H_2O absorption band (e.g. between ~1300–1400 cm^{-1}) that most of the channels in the 281 subset are located in the wings

Table I. AIRS 281 channel subset used here in terms of the original 2378 channels. Channels not used for any experiments are shown in italics.

1	6	7	10	11	15	16	17	20	21	22	24	27
28	30	36	39	40	42	51	52	54	55	56	59	62
63	68	69	71	72	*73*	*74*	*75*	*76*	*77*	*78*	*79*	*80*
82	*83*	*84*	86	92	93	98	99	101	104	105	108	110
111	113	116	117	123	124	128	129	138	139	144	145	150
151	156	157	159	162	165	168	169	170	172	173	174	175
177	179	180	182	185	186	190	192	198	201	204	207	210
215	216	221	226	227	232	252	253	256	257	261	262	267
272	295	299	300	305	310	321	325	333	338	355	362	375
453	475	484	497	528	587	672	787	791	843	870	914	950
1003	1012	1019	1024	1030	1038	1048	1069	1079	1082	1083	1088	1090
1092	1095	1104	1111	1115	1116	1119	1120	1123	1130	1138	1142	1178
1199	1206	1221	1237	1252	1260	1263	1266	1285	1301	1304	1329	1371
1382	1415	1424	1449	1455	1466	1477	1500	1519	1538	1545	1565	1574
1583	1593	1614	1627	1636	1644	1652	1669	1674	1681	1694	1708	1717
1723	1740	1748	1751	1756	1763	1766	1771	1777	1780	1783	1794	1800
1803	1806	1812	1826	1843	1852	1865	1866	1868	1869	1872	1873	1876
1881	1882	*1883*	1911	1917	1918	1924	1928	*1937*	*1941*	*2099*	*2100*	*2101*
2103	*2104*	*2106*	*2107*	*2108*	*2109*	*2110*	*2111*	*2112*	*2113*	*2114*	*2115*	*2116*
2117	*2118*	*2119*	*2120*	*2121*	*2122*	*2123*	*2128*	*2134*	*2141*	*2145*	*2149*	*2153*
2164	*2189*	*2197*	*2209*	*2226*	*2234*	*2280*	*2318*	*2321*	*2325*	*2328*	*2333*	*2339*
2348	*2353*	*2355*	*2357*	*2363*	*2370*	*2371*	*2377*					

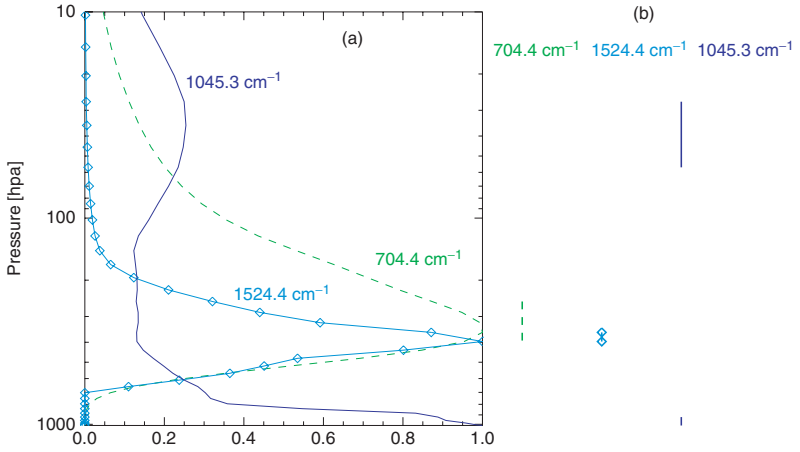

Figure 1. a) Normalized weighting functions for AIRS channels centred at 704.4, 1524.4, and 1045.3 cm^{-1}. b) Weighting function peaks and widths (see text for more explanation) for the same channels. This figure is available in colour online at www.interscience.wiley.com/qj

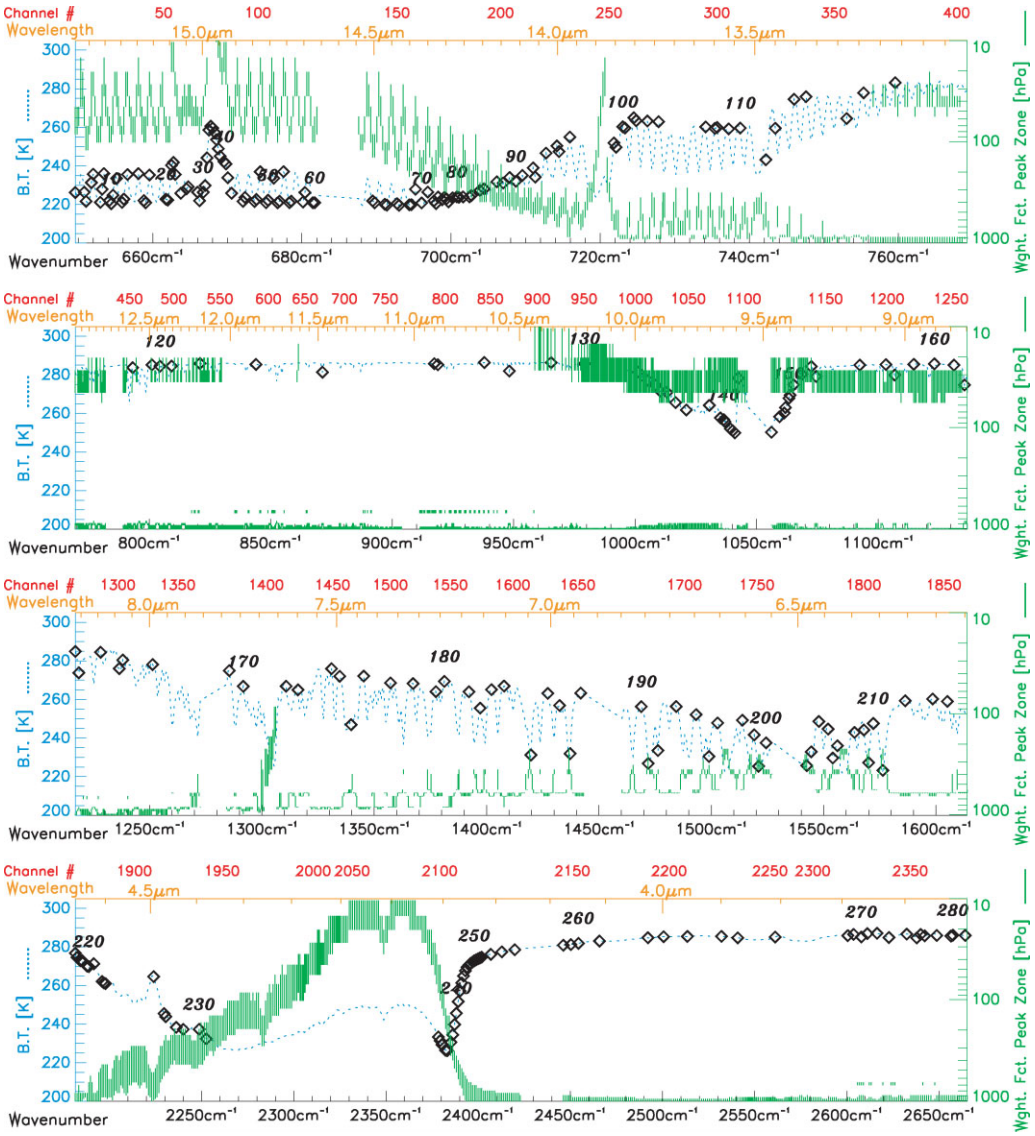

Figure 2. Simulated AIRS brightness temperature spectrum for a midlatitude profile (dotted line). ◊: channels from the 281 subset with channel numbers listed directly above. The top-most horizontal scale is the channel number in terms of the full 2378 channel set (labelled Channel #); The left hand scale is the brightness temperature (B.T.) in Kelvins; The vertical lines give the peaks and extents of the channel weighting functions in terms of pressure on the right hand scale as in Figure 1. This figure is available in colour online at www.interscience.wiley.com/qj

of absorption lines. These lines typically have sharper weighting functions than those near line centres. However, to include the highest peaking H_2O band channels, the subset also includes channels on the line centres of the strongest lines (e.g. near 1550 cm^{-1}). Also shown for reference are the weighting function peaks and widths for all channels.

There are nine AIRS pixels within a collocated AMSU-A footprint. This combination is known as a 'golfball'. In the cross-track direction, there are 30 golfballs (30 AMSU-A and 270 AIRS pixels). The AIRS and AMSU-A radiance data set used here retains half of the available golfballs (every other one). Several NWP centres currently receive or have received in the past only the centre AIRS pixel of a golfball. Other centres receive the warmest of nine pixels in a golfball. The data set used here is that received in NRT that includes all nine AIRS pixels within a golfball. This allows an evaluation of different methods of spatial data reduction.

3. The fvSSI Data Assimilation System

A data assimilation system (DAS) was used. It will be referred to as the fvSSI. The fvSSI uses the general circulation model (GCM) of Lin *et al.* (2004), called the fvGCM. The analysis system is the 3D variational (3DVAR) Spectral Statistical Interpolation (SSI) scheme developed at the National Centers for Environmental Prediction (NCEP) (Parrish and Derber, 1992; Derber and Wu, 1998).

This version of the SSI evolved from one that was operational circa 2004. It includes a few upgrades that are part of more recent SSI versions such as updated observational errors and radiative transfer for satellite radiances. It does not include other recent updates that have further improved forecast skills (see http://www.emc.ncep.noaa.gov/gmb/STATS/html/model_changes.html for more details).

The SSI was run with two outer loop iterations. During each of these iterations, the Jacobians (partial derivative of the observable with respect to the state variables) were linearized about the current state estimate. Following each outer loop iteration is the inner loop in which the gradient information, search direction, and step sizes were computed to update the analysis increments. One hundred iterations of this loop were allowed in this configuration.

The fvGCM consists of the finite volume (fv) dynamical core of Lin (2004) with NCAR CCM3 physics (Kiehl *et al.*, 1996). The gridpoint fvGCM is run at a horizontal resolution of 1° latitude $\times$1.25° longitude in both forecast and data assimilation modes. The model has 55 layers with the top at 0.01 hPa. In order to conduct a relatively large number of experiments, a lower horizontal resolution was used for the analysis (T62L64: spectral triangular truncation of 62 ($\sim$200 km) and 64 vertical levels) than the operational NCEP analysis system. Note that the top level of the SSI (0.266 hPa) is not as high as the GCM model top.

The input observations consist of most of the data that were operationally assimilated at NCEP during the time-period evaluated here: January 2003. These include conventional data such as radiosonde temperatures, humidities, and winds. Cloud-track, water vapour, and ocean surface winds from several satellites were used. In addition, fvSSI assimilates ozone retrievals from the NOAA 16 Solar Backscatter Ultraviolet (SBUV) radiometer. NCEP's operational system includes precipitation assimilation, whereas the fvSSI does not.

This system also assimilates brightness temperatures from the NOAA 14 High Resolution Infrared Sounder 2 (HIRS-2) and MSU, NOAA 15 AMSU-A and AMSU-B, NOAA 16 HIRS-3, AMSU-A, and AMSU-B, the Geostationary Operational Environmental Satellite (GOES) 8 and 10 sounders, and the NASA EOS Aqua AMSU-A and AIRS as described in McNally *et al.* (2000) and Derber and Wu (1998). AIRS data are currently assimilated operationally at NCEP, but were not in January 2003. Brightness temperatures were computed within the DAS using the Community Radiative Transfer Model (CRTM), formerly known as OPTRAN (Kleespies *et al.*, 2004).

The radiance bias correction scheme is adaptive and includes scan-position-dependent corrections for each channel of every instrument. The initial bias correction coefficients for all channels were set to zero at the beginning of the experiment. A time constant parameter was then specified to control how quickly the system adjusts to the computed bias corrections. A value of two days was used to obtain a relatively rapid response to the observations while not allowing substantial fluctuation in the derived coefficients over adjacent synoptic periods.

One relatively new feature of the SSI analysis system is the cloud detection scheme used for radiance data. This scheme finds a cloud fraction and cloud top pressure that best agree with the radiance data from an individual sounding. The cloud fraction and cloud top pressure were estimated during each of the two outer loop SSI iterations. Therefore, the cloud properties were estimated once before the initial inner loop analysis. They were then updated after the first inner loop analysis of temperature, humidity, ozone, and surface skin temperature. The inner loop analyses use only those channels that were determined to be insignificantly affected by clouds (i.e. channels for which the computed cloud effect is less than 0.2K). This allows the DAS to potentially use many unaffected AIRS channels in a cloudy pixel.

4. Experimental setups

Table 2 gives a summary of the names and parameters for all experiments. The aim is to check the analysis and forecast sensitivity to changes in the channel errors, the channel selection, and the type of spatial subsetting applied. The following subsections provide an explanation of the experimental parameters.

Table II. Experimental setup (see text for more details). Alternate experiment names are given in parentheses. The last four columns list the number of channels falling within the given spectral ranges.

Experiment name	AMSU used	Spatial subset	AIRS chan. errors	H_2O cycled	650-920 cm^{-1}	920-1080 cm^{-1}	1080-1610 cm^{-1}	2180-2242 cm^{-1}	650-2242 cm^{-1}
No AIRS/AMSU	No	–	–	Yes	–	–	–	–	–
AMSU	Yes	–	–	Yes	–	–	–	–	–
AIRS	No	warmest	small	Yes	115	29	0	12	156
No H_2O (Small) (Warmest FOV)	Yes	warmest	small	Yes	115	29	0	12	156
No H_2O, no O_3	Yes	warmest	small	Yes	115	0	0	12	127
H_2O (Small)	Yes	warmest	small	Yes	115	29	59	12	215
No H_2O Large†	Yes	warmest	large	Yes	115	29	0	12	156
H_2O^* Large	Yes	warmest	large	Yes	85	4	49	14	152
Centre FOV	Yes	centre	small	Yes	115	29	0	12	156
No cycle H_2O	Yes	warmest	small	No	115	29	59	12	215

† Only 19 forecasts available.

4.1. EOS Aqua channel selection and assigned channel errors

Each AIRS (or other sounder) channel is assigned a constant brightness temperature (T_B) error for a given experiment. The specified channel errors affect the SSI analysis in two important ways. Firstly, they determine how much weight a particular channel will receive. Secondly, a strict quality control check (henceforth referred to as the background check) is performed whereby an observation is not used if the absolute value of the observed minus background (referred to as O-B) T_B is greater than either three times the specified error standard deviation or 4.5K. For example, if we want to give less weight to a particular channel by increasing the error, we must consider that more data from the channel will enter the analysis owing to the larger background check threshold (for channels with errors up to 1.5K). This could potentially allow more cloud-contaminated data into the analysis.

Experiments were conducted with two different sets of channel errors shown in Figure 3. The selected channels and their errors were chosen empirically based loosely on our experience with O-B statistics and other experiments not shown here. The first channel error set, referred to as Small, uses errors of approximately 0.3K for channels between $\sim$700 and 1000 cm^{-1}. Slightly larger errors are given to channels in the long-wave CO_2 band with $\nu <\sim 700$ cm^{-1} and those in the short-wave CO_2 band ($\nu >\sim 2180$ cm^{-1}). Channels were assigned in the H_2O band 2K errors. The second set, called Large, has errors of 0.7K in the 690–1300 cm^{-1} range with 2.5K errors in the H_2O band. In the short-wave CO_2 band, the Large channel errors are very similar to those of Small.

Using these two sets of channel errors, experiments were conducted with different selections of channels. Note that this can be thought of as a limiting case of varying the channel errors (such that the channels receive zero weight or are completely rejected by quality control thresholds). The aim is to check for potential aliasing of water vapour and ozone signals in the H_2O and O_3 bands, respectively, into temperature increments. To this end, all channels in the H_2O band between 1080 and 1610 cm^{-1} (shown as thick squares plotted at 0 K in Figure 3) in the experiment called No H_2O Small were eliminated. In addition to those, the experiment called No H_2O, no O_3 also discards O_3 band channels between 920 and 1080 cm^{-1} as indicated by the thin squares.

The channel selection was not optimal as there is some inconsistency between some of the experiments using the two error sets. For example, one of the experiments that used the Large errors (H_2O^* Large) discards channels between 990 and 1240 cm^{-1} as well as a few channels near 700 cm^{-1} and several of the channels that peak near the tropopause between 650 and 680 cm^{-1}. The experiments with the Small error set do not use 2 channels in the 2180–2190 cm^{-1} window that were moderately affected by carbon monoxide (CO) absorption. CO is assumed to have a fixed concentration in the CRTM. We do not believe that these channel selection differences affect the overall conclusions drawn from the experimental results based on a limited set of experiments not shown here.

Channels in the strongest part of the long-wave CO_2 band near 667 cm^{-1} were not used in any of the experiments. These channels have weighting functions that peak in the upper stratosphere with tails in the mesosphere above the highest SSI level. In this work, all channels in the short-wave CO_2 band with $\nu > 2242$ cm^{-1} were also discard. These include either somewhat redundant window channels and CO_2-sensitive channels that may have somewhat larger uncertainties in spectroscopy, sensitivity to frequency specification, and/or sensitivity to the atmosphere above the highest analysis level as compared with longer wavelength channels. In addition, some of the short-wave CO_2 channels were affected by reflected solar radiation and/or non-local thermal equilibrium (non-LTE) during the day (Strow *et al.*, 2006).

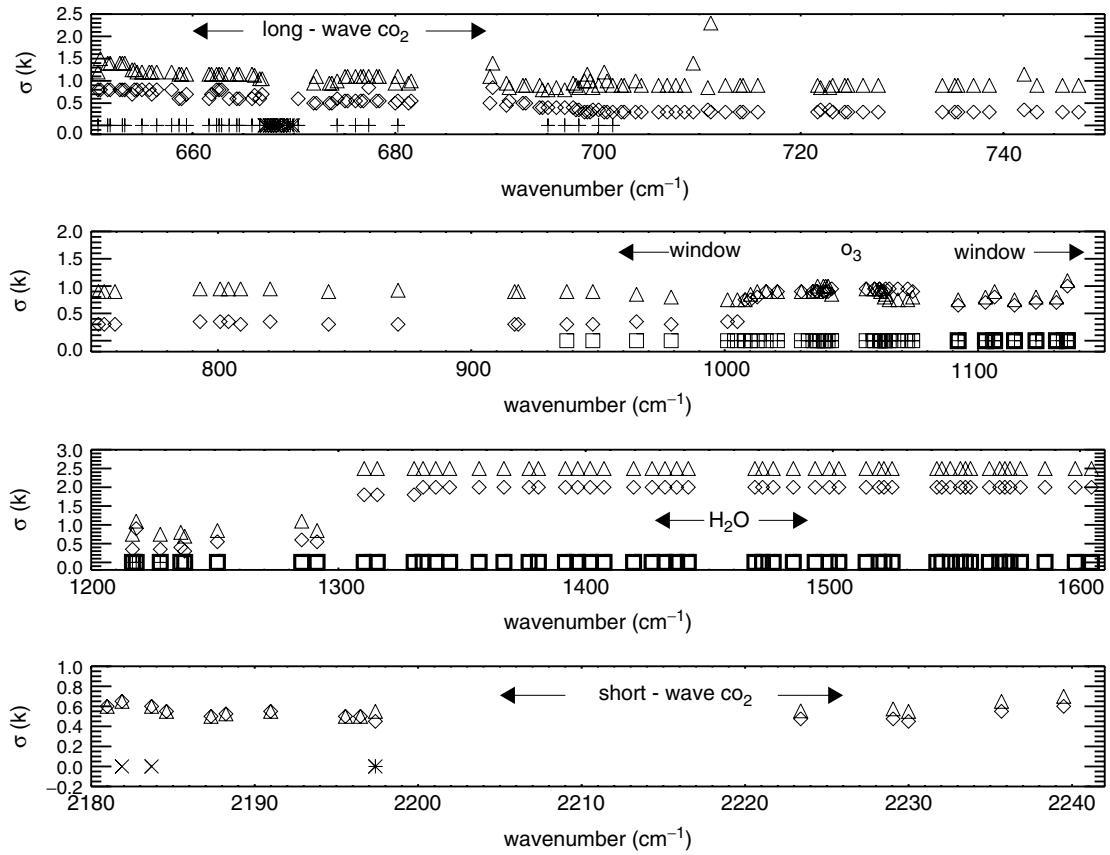

Figure 3. Assigned brightness temperature errors for AIRS channels. △: Large error set; ◊: Small error set; Channels not used in given experiments are shown as having zero error. ×: not used in Small set; +: not used in H_2O* large; thick squares: not used in No H_2O (Small and Large); thin square: not used in No H_2O, no O_3 (in addition to thick squares). Major absorbers and band characteristics are indicated.

For the EOS-Aqua AMSU-A, channel 7 is not used due to excessive noise. In addition, as with all other AMSU-A instruments, channel 14 is not used. This channel is sensitive to temperature in the upper stratosphere and mesosphere above the highest SSI level.

4.2. Spatial subsetting

Assimilation experiments with two different methods of spatial subsetting were performed. Specifically, one of the nine AIRS fields-of-view (FOV) within a golfball were chosen by selecting either the centre FOV or the warmest FOV (as defined by the brightness temperature in the 917.1 cm^{-1} channel). The advantage of the centre FOV selection is that it potentially simplifies the across-track bias correction, because the same scan positions will be used for all scan lines. The warmest FOV selection can potentially find more holes in the clouds. However, the warmest FOV procedure does not always ensure that the most channel data for a given golfball will be used or that the least cloudy pixel will be selected. For example, a high cloud with either a low emissivity or low cloud fraction may produce a warmer T_B in a window channel than a lower cloud with a higher emissivity/cloud fraction. A temperature inversion may produce cloudy T_B observations that are warmer than surrounding clear ones.

Figure 4 shows T_B observations and differences between the warmest and centre FOV spatial subsettings for a temperature sounding channel whose weighting function peaks near 780 hPa. The largest differences occur in cloudy regions. These are precisely the areas where forecasts may have a large sensitivity to AIRS data (McNally, 2002; Fourrie and Rabier, 2004). The mean T_B difference between the two data sets is significant at more than 2K. The standard deviation is also large (over 4K). Mean T_B differences range from 0.28–4.4 K for temperature-sensing channels whose weighting functions peak between ∼240 hPa and the surface, respectively.

5. Results of AIRS assimilation experiments

5.1. Data coverage and O-B statistics

Figure 5 shows the percentage of the thinned data that pass the cloud detection and background checks for the warmest FOV (Small and Large errors) and centre FOV (Small errors). The statistics were computed for 06Z on 20 December 2002. Both the spatial subsetting and the specified channel errors play significant roles in determining how much data enters the analysis. As expected, the warmest FOV subsetting allows more data to enter the analysis for channels peaking in the lower troposphere that are affected by cloud. Changing the

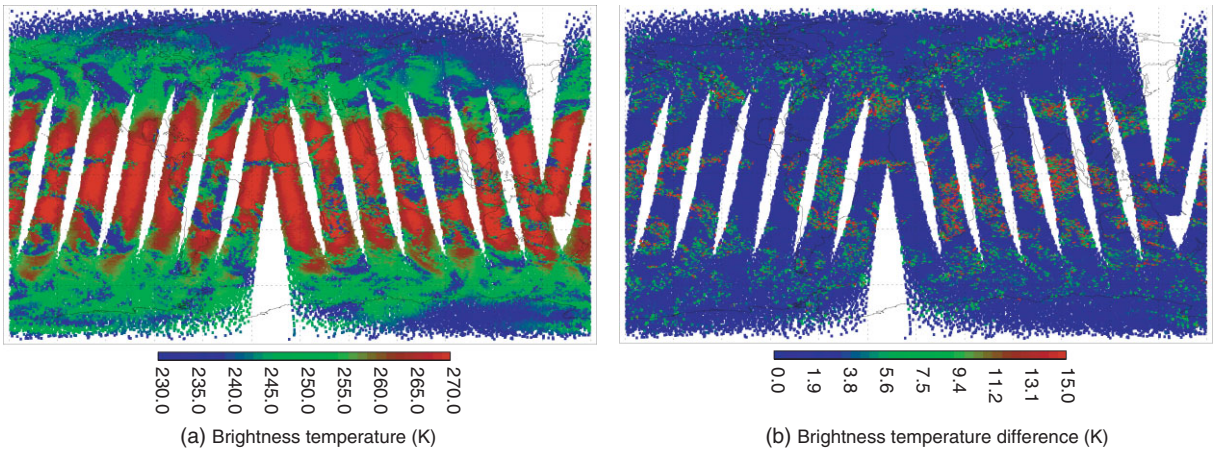

Figure 4. a) Observed brightness temperatures for AIRS channel centred at 738.6 cm^{-1} for 20 December 2002, 03Z-15Z, centre FOV subsetting. b) Difference between warmest and centre FOV.

channel errors can have an even larger effect on the amount of data accepted by the analysis owing to the fact that the errors determine the thresholds for the background check.

Figure 6 similarly shows global O-B statistics for the same three experiments. The method of spatial subsetting has little effect on either the O-B means or standard deviations. Even though the centre-FOV observations are cooler on average (for the entire AIRS population), the O-B statistics for the two spatial subsets are similar because a smaller population of AIRS pixels is determined to be clear for the centre-FOV case. However, the specified channel errors do have a significant effect on the O-B statistics, particularly the standard deviation for channels with $\nu < 1000$ cm^{-1}. This is expected as the channel errors affect the background check thresholds. Note that there is no difference in standard deviations in the H_2O band. Because the background check threshold is capped at 4.5K, which is less than 3σ for these channels, changing the channel errors from 2 to 2.5K did not impact the quality control decisions. For the lowest peaking channels in the longwave window, the bias is larger and more negative when using the Large channel errors. This could be an indication that more cloud-contaminated data enters the system when the Large channel errors were specified.

Figure 7 shows maps of O-B and coverage for 12 hours of observations (the same time period as in Figure 4). This shows data for the 704.4 cm^{-1} CO_2 band channel and for the 1524.4 cm^{-1} H_2O band channel. These channel weighting functions can peak at similar pressures (~350 hPa). As shown in Figure 5, more observations (~10%) are accepted in the warmest FOV subsetting (Figure 7b) as compared with the centre FOV subsetting (Figure 7a) mostly at the edges of cloud-covered areas and in partly cloudy regions. An illustration of this is seen over southern Africa.

There is a large increase in the number of accepted observations (~40%) when the Large errors are used (Figure 7b–c). We have observed similar increases of 30–40% on other randomly selected days. Frequently, more data are accepted with the Large errors over Africa and Australia. This may be the result of errors in the background skin temperature and/or undetected cirrus as will be discussed in the next subsection. The increase in accepted observations is especially apparent at high latitudes. In the northern high latitudes, the O-B tends to be positive which is inconsistent with cloud-contamination. As this situation is repeated on other days at different locations, it may be the result of model error (bias). At southern high latitudes, O-B is more often negative. Figure 4 indicates that these latitudes can be frequently cloud-covered, although this channel may sometimes be unaffected by low cloud. It is difficult to determine from this figure whether cloud-contaminated data are entering the analysis.

Even more observations from the 1524.4 cm^{-1} H_2O band channel enter the analysis (Figure 7d) as compared with the 704.4 cm^{-1} CO_2 band channel whose weighting function peaks at a similar altitude. Reasons for this include the different error specifications that affect the background check and the fact that the 1524.4 cm^{-1} weighting function is more variable and narrow (see Figure 1) so that it may more frequently be unaffected by low clouds. For example, there is better coverage over low clouds in the middle and high southern latitudes. The O-B for this channel shows smaller-scale structure presumably due to background humidity errors.

5.2. Cloud detection

Here, we compare the analysed cloud-top pressures with those from the EOS Aqua Moderate-Resolution Imaging Spectroradiometer (MODIS). The MODIS cloud-top pressures are derived using a CO_2 slicing technique within 1km diameter pixels (Menzel and Strabala, 1997). We use the MODIS cloud-top pressure contained in the level-3 atmosphere product (MOD08) collection 4 (King *et al.*, 2003). The level-3 data are statistics (e.g. mean, minimum, maximum) that are sorted into 1° latitude $\times$1°

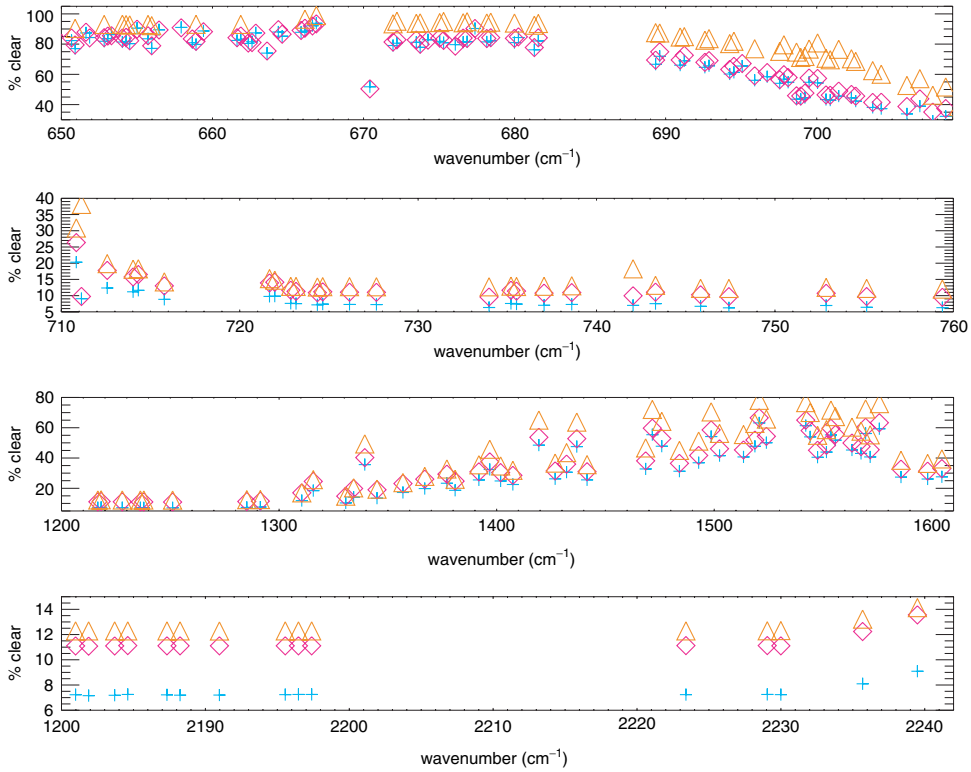

Figure 5. Percentage of thinned AIRS data that pass the analysis cloud detection and quality control checks: △: warmest FOV, H_2O Large; ◊: warmest FOV, No H_2O Small; +: centre FOV, No H_2O Small. Some channels are shown as if they had been used in the analyses, but were not actually used. Other channels are omitted as their data counts are similar to channels shown. This figure is available in colour online at www.interscience.wiley.com/qj

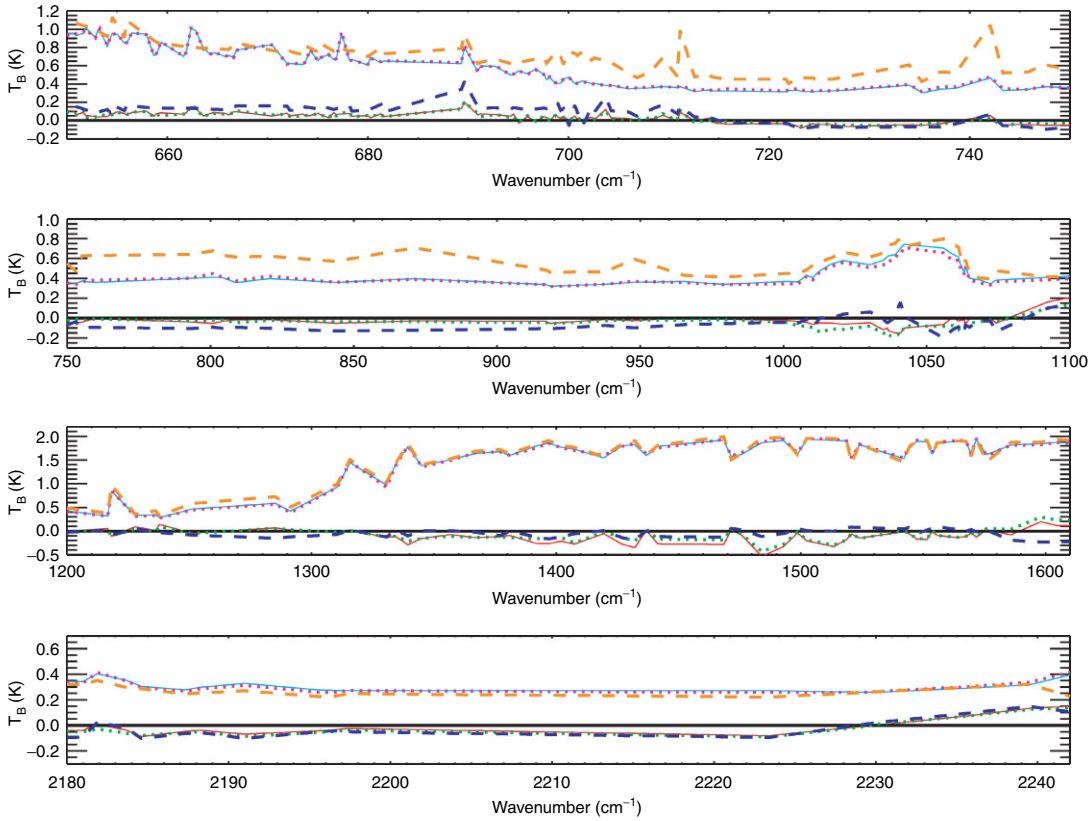

Figure 6. As in Figure 5 but showing globally-averaged O-B statistics: Mean (lower set of lines near the thick solid zero line) and standard deviations (upper set of lines). Thin solid: Warmest FOV (No H_2O Small); Dotted: centre FOV (No H_2O Small); Dashed: H_2O Large (Warmest FOV). This figure is available in colour online at www.interscience.wiley.com/qj

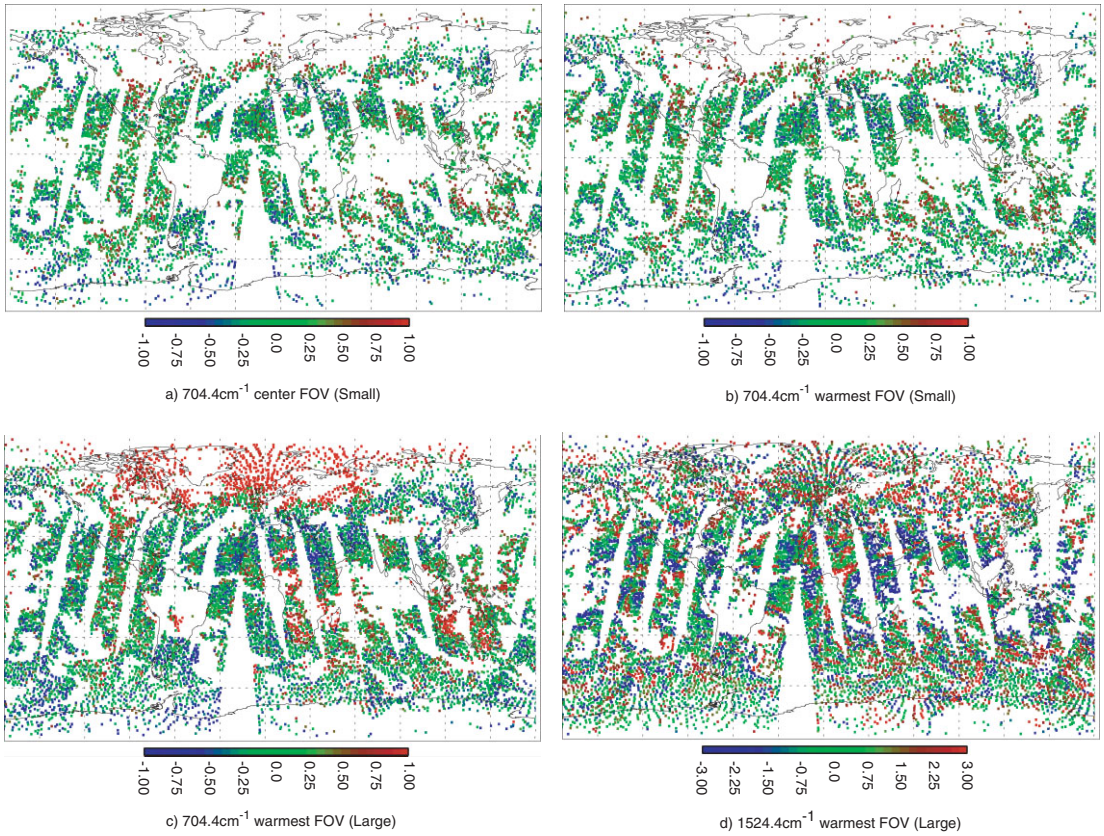

Figure 7. a) O-B for AIRS channel at 704.4cm^{-1} for 20 December 2002, 03Z-15Z, centre FOV subsetting (No H_2O Small); b) Same as a) but warmest FOV subsetting; c) Same as b) but for H_2O* Large; d) Same as c) but AIRS channel at 1524.4 cm^{-1} (note different scale) .

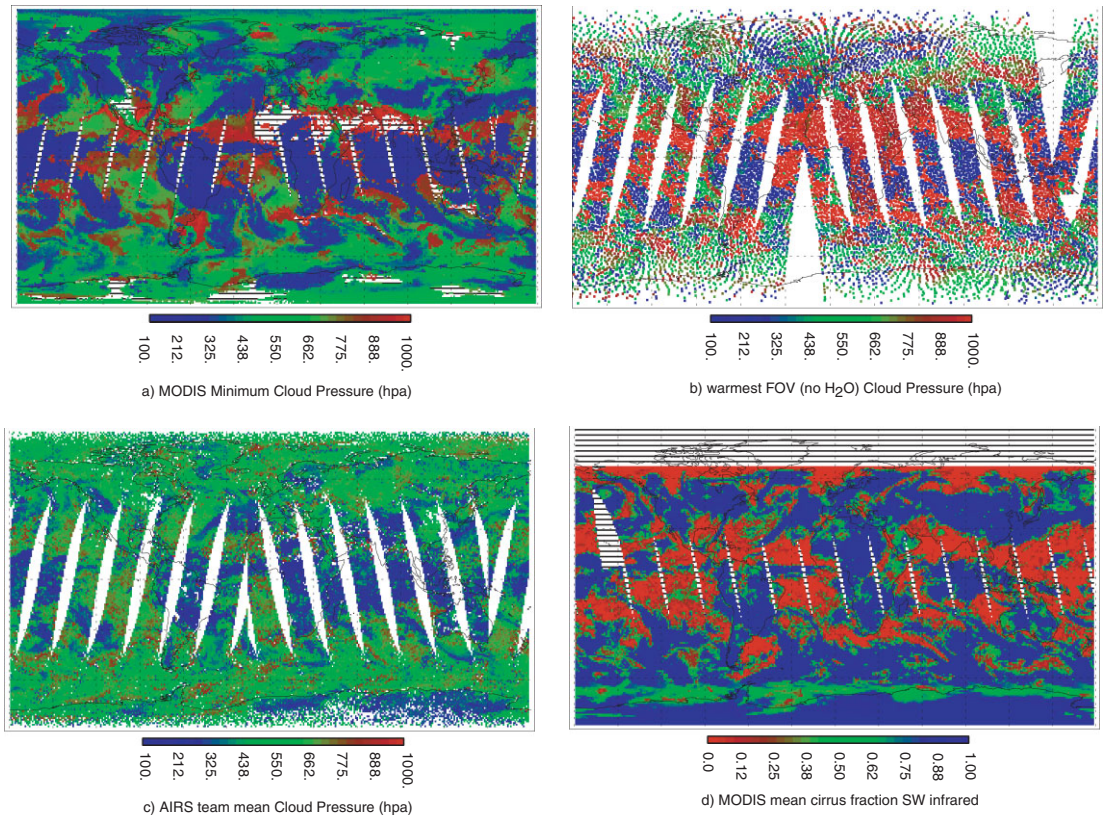

Figure 8. Cloud parameters for 20 December 2002: a) MODIS gridbox minimum cloud pressure; b) cloud pressure from fvSSI DAS (03-15Z); Cloud pressures are shown as the surface pressure where the cloud fraction was zero; c) AIRS science team gridbox mean cloud pressure; d) cirrus fraction from MODIS (day orbits only). Hatched areas in a) and d) indicate gridboxes with either no observations or where the cloud fraction was zero (in a) .

Published in 2007 by John Wiley & Sons, Ltd.

Q. J. R. Meteorol. Soc. **133**: 181–196 (2007)
DOI: 10.1002/qj

longitude cells on an equal-angle global grid. The cloud-top pressures are separated into daytime only, night-time only, or combined day and night. Here, we use the separate products to match up orbits with AIRS. At latitudes above 60°, we use the combined day-night data set.

Figure 8a–c shows the MODIS minimum, fvSSI, and AIRS science team level 3 (Aumann *et al*., 2003) cloud pressures, respectively. Examination of the MODIS gridbox maximum cloud pressures reveals a significant incidence of multiple cloud decks within a gridbox. AIRS may or may not be able to see through holes in the upper cloud deck as its spatial resolution is significantly poorer than the MODIS 1 km^2 pixels. The AIRS science team gridbox mean cloud pressures look very similar to the MODIS minimum cloud pressures although they appear to have more spatial variability. The AIRS team product shows less incidence of low clouds everywhere. It also has somewhat higher pressures for frontal clouds at high latitudes similar to fvSSI cloud pressures.

The fvSSI generally does a good job of differentiating between deep convective clouds in the tropics and lower frontal clouds at middle and high latitudes. The success of the cloud detection algorithm is less certain over very warm land surfaces such as in the southern desert areas of Africa and Australia. AIRS data over these areas represent local summer daytime conditions. The brightness temperatures over much of southern Africa and Australia were extremely high, often in excess of 320K indicating very high surface skin temperatures. MODIS short-wave (SW) infrared channels indicate high fractions of cirrus cloud (Figure 8d) over these locations while the fvSSI sometimes finds either no or low clouds. Both the AIRS team product and that from the spatial variability approach of Joiner *et al*. (2004) (not shown) also indicate the presence of high clouds over these areas.

Joiner *et al*. (2004) explained a potential difficulty in using an O-B-type approach for cloud detection in such areas. A background error in the surface skin temperature can offset cloud effects in O-B. This may result in a cloud-contaminated observation passing cloud-detection checks. Such errors are quite possible when surface skin temperatures are extremely high (e.g. background skin temperatures are too low). Note that a cirrus/low-cloud check involving the differences between long- and short-wave window channels has been added to more recent SSI versions (Le Marshall *et al*., 2006), but was not included in this version.

We find that the incidence of pixels identified as clear by the SSI was ∼28% (21)% for the warmest(centre) FOV selection. Chahine *et al*. (2006) find that less than 1% of AIRS pixels are cloud free to the instrument noise level. Therefore, it is likely that some cloud contaminated AIRS data enters the analyses.

5.3. Forecast skill

All experiments began with a two week spin-up period in mid-December 2002. The forecasts were run daily for January 2003. The forecast results for each experiment were verified against the operational NCEP analyses at 2° × 2.5° resolution. This may slightly penalize the results with AIRS data as they were not assimilated at the time. The forecast anomaly correlation scores include all waves. The extratropical scores were averaged (area weighted) over latitudes from 30° to 86°. A summary of all the scores is given in Table 3 along with confidence levels for the differences between relevant pairs of experiments.

5.3.1. Channel selection

Figure 9 shows forecast anomaly correlation scores for four experiments. The first uses neither AIRS nor EOS AMSU-A data, and three others use EOS AMSU-A with different AIRS channel selections. All experiments with AIRS data have a positive impact in the northern hemisphere as compared with No AIRS/AMSU. No H_2O Small has the largest impact. In the southern hemisphere, No H_2O Small also has the largest positive impact, while H_2O Large has a slightly negative impact.

We find that removing O_3 band channels in addition to the H_2O-band channels had little effect. Using the Large errors compared with the Small similarly had little impact on forecast skill even though this had a significant impact on the amount of data accepted by the analysis. Note that we have a somewhat smaller sample for the No H_2O Large experiment. This sample was compared to the same from AMSU and No H_2O Small to generate the confidence levels in Table 3.

We see from these experiments that the inclusion of channels in the H_2O band slightly degrades the AIRS impact in our current experimental setup. This degradation could be the result of one or more effects. Firstly, if the GCM has significant biases in the humidity field, then assimilating good humidity information may actually degrade the analysis (Chen *et al*., 1999) by, e.g. producing excessive convection and precipitation.

Secondly, channels in the H_2O band have a large sensitivity to both temperature and humidity. These channels also have very sharp weighting functions and may enter the analysis more often than similarly peaking CO_2 channels over low clouds and as a result of having larger errors that allows more data in through the background check. If the background errors for temperature and humidity are misspecified, this may result in incorrect partitioning of temperature and humidity increments for a given brightness temperature innovation.

Finally, channels may cause degradation if the cloud detection or quality control thresholds are inadequate or if the bias correction scheme is insufficient to account for systematic errors in the forward model or observations themselves. Section 6 focuses on the first two of these underlying effects of the H_2O band channels.

5.3.2. Instrument selection

Figure 10 examines the impact of the AIRS (No H_2O Small from above) and the EOS Aqua AMSU-A separately and together as compared with an experimental run

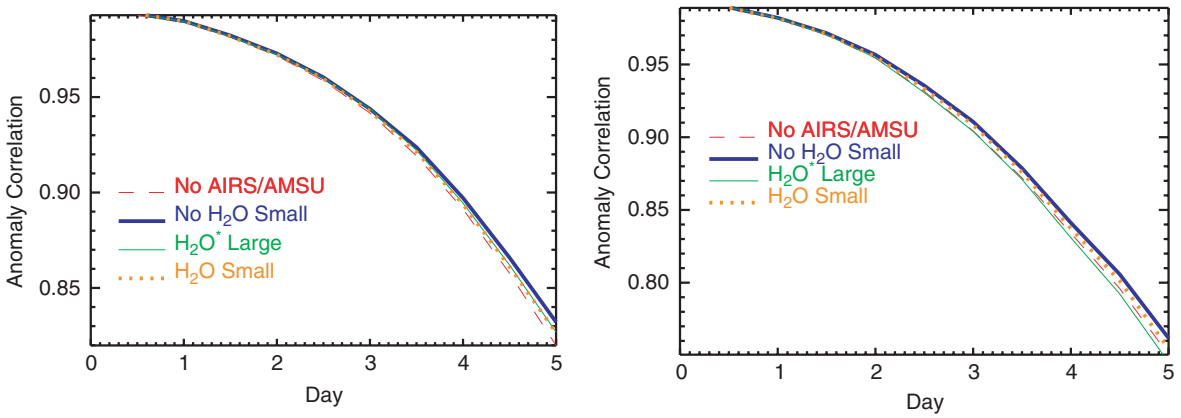

Figure 9. 31 day average of forecast 500 hPa anomaly correlation for northern (left) and southern (right) hemispheres. This figure is available in colour online at www.interscience.wiley.com/qj

Table III. Summary of 5-day 500 hPa geopotential height anomaly correlation (AC) scores for the northern and southern hemispheres (NH, SH, respectively) and the statistical confidence levels (in %) for differences with AMSU (C1) and no H_2O Small (C2). Statistically significant results (to the 90% level) are shown in italics.

Exper-iment	AMSU	no H_2O small	H_2O small	H_2O^* large	no H_2O no O_3	no H_2O large	no AIRS AMSU	AIRS	centre FOV	no cycle
AC NH	0.824	0.833	0.828	0.830	0.831	0.821†	0.821	0.829	0.833	0.824
AC SH	0.764	0.763	0.757	0.750	0.760	0.780†	0.754	0.749	0.757	0.760
C1 NH	–	*98.5*	64.6	*93.8*	*96.6*	99.9†	72.9	71.3	*99.3*	4.9
C1 SH	–	5.7	73.7	*95.0*	40.2	21.6†	*93.9*	*93.1*	81.1	34.4
C2 NH	*98.5*	–	*98.4*	79.2	*94.6*	4.9†	*99.5*	*90.9*	3.4	*99.4*
C2 SH	5.7	–	*95.5*	*90.4*	70.2	65.9†	75.9	*99.5*	82.5	46.2

† 19 forecasts.

that uses neither AIRS nor EOS-AMSU-A. In the northern hemisphere, AIRS gives a positive impact without the EOS-AMSU-A. AIRS provides a larger impact separately than the EOS-AMSU-A. In this hemisphere, the use of both instruments together provides a larger positive impact than the sum of the two alone. The results are somewhat different in the southern hemisphere. Here, the EOS-AMSU-A provides a positive impact while AIRS alone gives a neutral impact. The addition of AIRS to the EOS-AMSU-A does not yield significant improvement in this hemisphere.

It should be noted that there is some redundancy in the orbits of the EOS Aqua and NOAA-16. Therefore, the impact from the EOS Aqua AIRS/AMSU-A combination may be somewhat less than if it were in a completely independent orbit.

5.3.3. *Spatial subsetting*

As shown above, the method of spatial subsetting had a significant effect on the amount of data ingested into the analysis. There are indications of improvement using the warmest FOV selection in the southern hemisphere with a confidence level of about 80%. However, this is not generally considered to be a statistically significant result.

6. Discussion

In order to examine the effect of interaction between the moisture analysis and the model physics, we reconfigured our data assimilation system to analyse humidity as usual (with all satellite instruments), but then to not feed back the analysed moisture field to the model. This allows humidity-sensitive channels in the long-wave CO_2 band to have the potential benefit of a simultaneous moisture analysis with all other instruments. At the same time, the possibility of negative interaction between the humidity analysis and the model physics is eliminated. The model essentially runs with its internally-generated humidity field.

We ran the system in this configuration (called No cycle H_2O) with the same channel set as in H_2O Small. We find in Table 3 that the hemispherically-averaged 5-day forecast skills are very similar to those in the standard configuration with the same AIRS channel set (H_2O Small). Given this result, it is likely that other factors are contributing to the degradation of skill stemming from the use of channels in the H_2O band.

In order to isolate the effect of the H_2O band channels on the temperature analysis, we ran a set of experiments with combinations of only AIRS and EOS AMSU-A channels (i.e. no other data). We examine only the first analysis from these experiments on 17 December 2002.

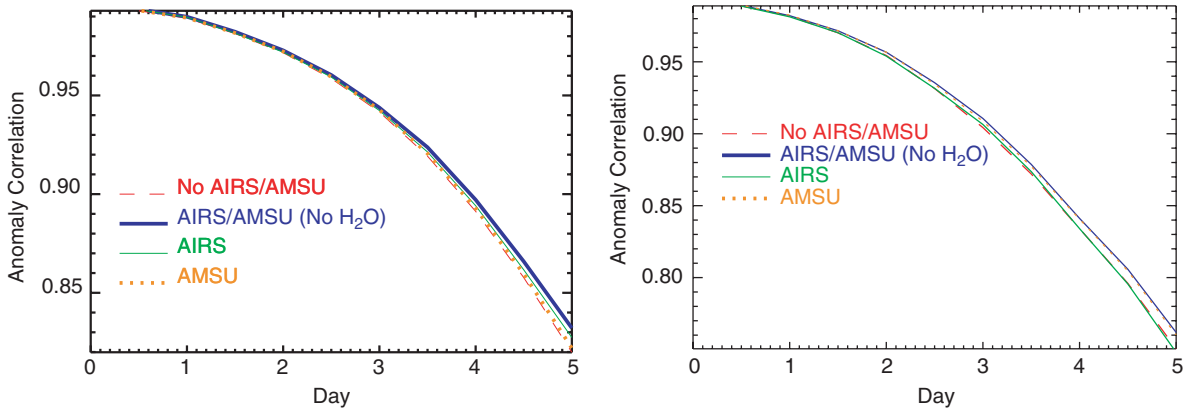

Figure 10. Similar to Figure 9 but for AIRS (no H_2O small) and AMSU-A combination experiments. This figure is available in colour online at www.interscience.wiley.com/qj

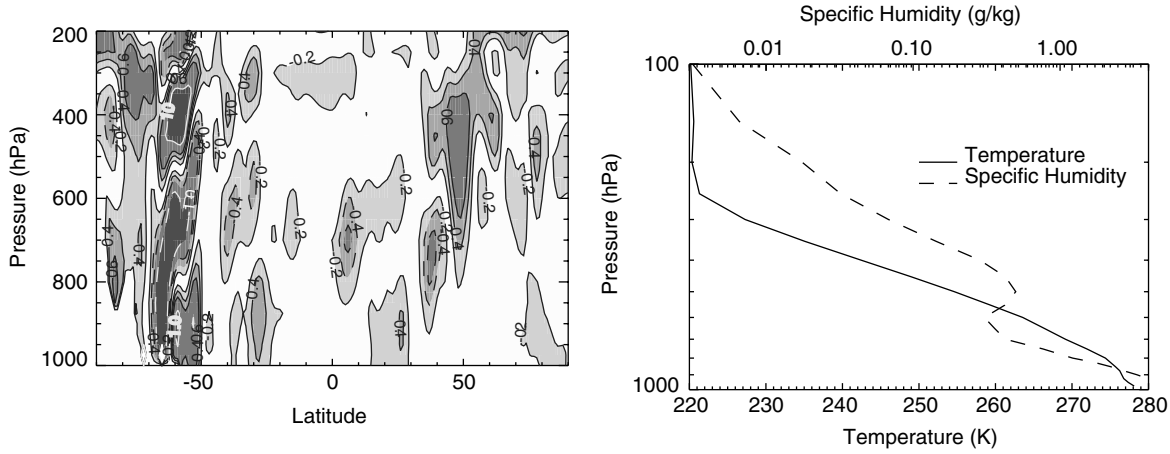

Figure 11. Left: Cross-section through 122.5 °W of temperature increments (K) produced by H_2O band channels. Contour lines have 0.2K increments (differences > 1K shown as 1K); Dashed line: Negative contours. Right: Background temperature and specific humidity at 60 °S, 122.5 °W.

Figure 11 shows a cross-section through 122.5 °W longitude of the difference in temperature increments between analyses with and without H_2O channels. Both experiments use EOS-AMSU-A data and the channel selection and errors of H_2O and No H_2O Small. The largest differences in temperature increments are at middle to high latitudes. Around 60 °S, an oscillating vertical pattern is present. There were a number of clear soundings near this gridbox where the analysis ingested all of the AIRS channel data. The background temperature and specific humidity profiles for 60 °S, −122.5 °W are also shown in Figure 11.

Figure 12 shows temperature and specific humidity increments at this location for four different channel configurations as well as differences in increments with respect to the experiment with all AIRS (no AMSU-A) channels. AMSU-A is seen to have a relatively small effect on both the temperature and humidity increments. In contrast, the H_2O band channels have a relatively large effect on temperature increments. The overall structure of the temperature increments with all AIRS channels is similar to that produced using only H_2O band channels and contrasts significantly with the increments generated without those channels. The magnitude of the differences in temperature increments (±1.5K) produced by the H_2O band channels is quite significant in this case.

Figure 13 shows spectra of T_B computed from the model and O-B for a sounding determined to be cloud free that influenced the increments shown above (at −60.55 °S, −121.61 °W). The generally negative values of O-B near 666 cm^{-1} produce cooling near and above the tropopause (∼200 hPa) as shown in the temperature increments of Figure 12. Positive O-B values for $\nu >\sim 750$ cm^{-1} produce warming in the lower troposphere.

O-B values in the H_2O band are positive(negative) for the channels with strong(weak) H_2O absorption. The negative(positive) O-B values should produce an increase(decrease) in water vapour and/or a cooling (warming) in the lower(upper) troposphere. The primary effect of the H_2O band O-B statistics on the increments is an increase in humidity peaking near 700 hPa. When H_2O band channels are removed from the analysis, other channels with less humidity sensitivity (e.g. in the long-wave window) produce a much smaller increase in humidity around 700 hPa, and the warming at this altitude is less.

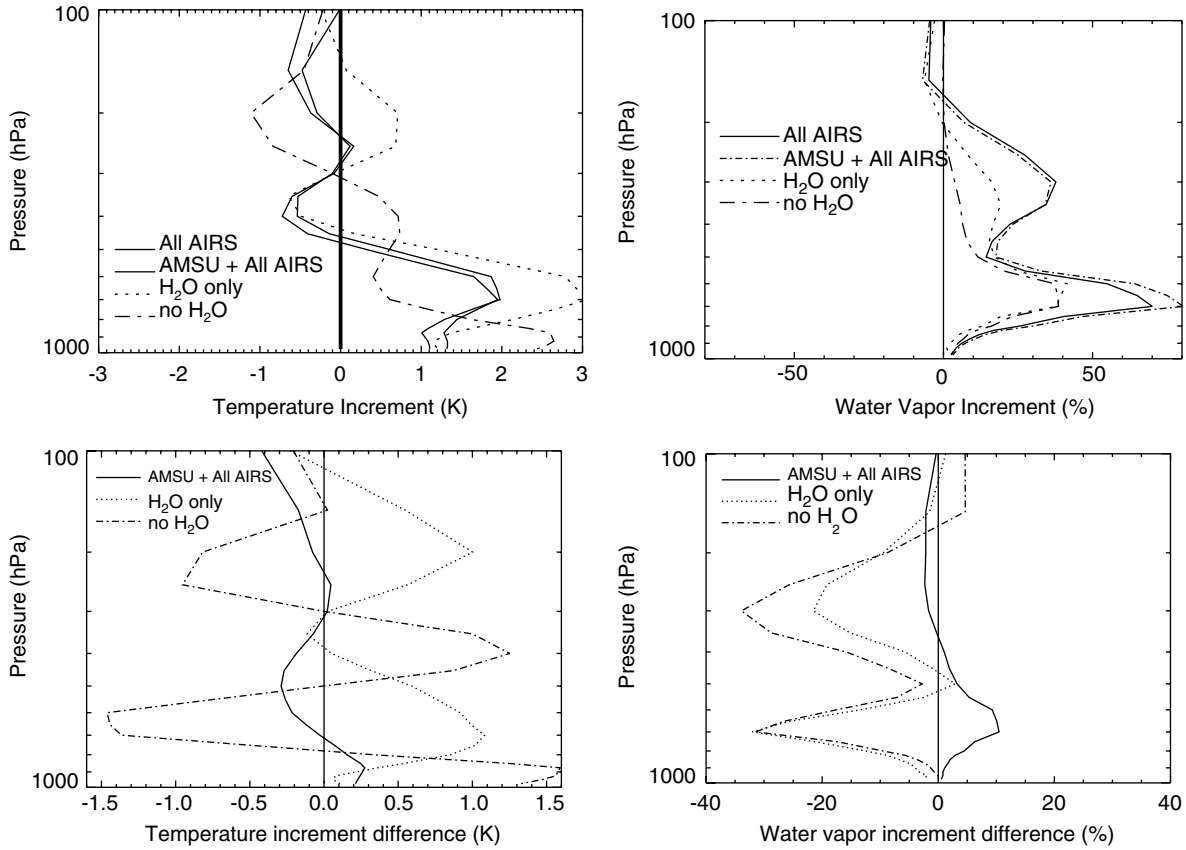

Figure 12. Top left: Temperature increments at 60 °S, 122.5 °W; Top right: As in top left but for specific humidity; bottom left: Difference in temperature increments with respect to All AIRS; bottom right: As in bottom left but for specific humidity.

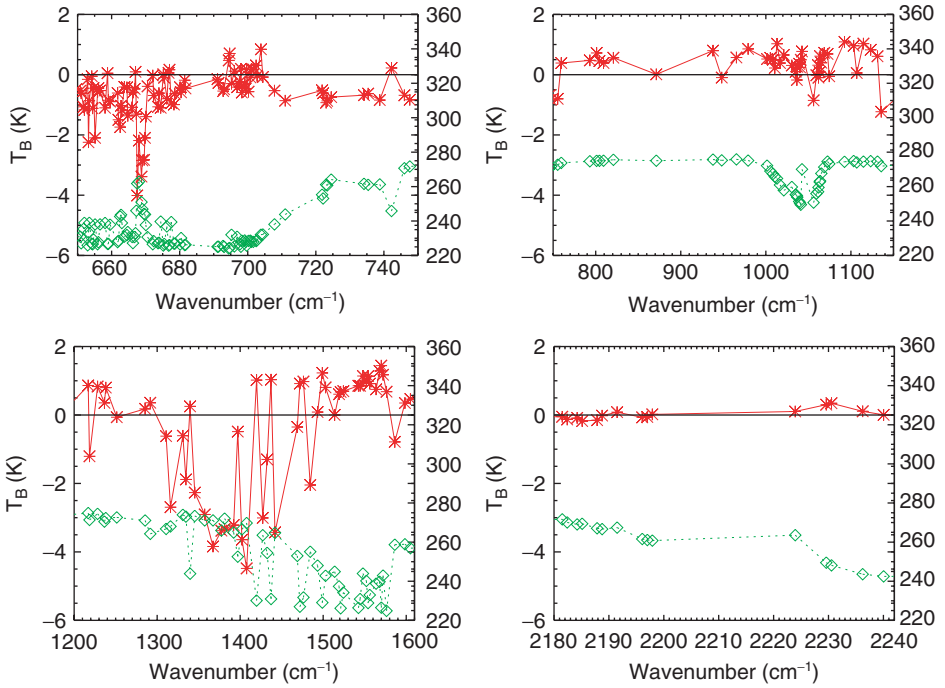

Figure 13. Brightness temperatures computed from the model (dotted line with diamonds, right scale) and O-B (solid line with stars, left scale). The zero line is shown for reference as a thick solid line. This figure is available in colour online at www.interscience.wiley.com/qj

The vertical oscillations in the temperature increments resulting from the H_2O band channels are produced by a complex relationship between background errors and the O-B spectra that is not readily apparent from the O-B spectra alone. We do not know exactly where the truth lies in this case. Information content studies show that H_2O band channels do provide useful information about temperature as well as humidity and complement information from the CO_2 bands (e.g. Rabier *et al*., 2002). However, based on our forecast skill scores, this information may be incorrectly partitioned in our DAS.

To make use of the information content in the H_2O band, background errors as well as observation errors have to be correctly specified. Both the background error variances and vertical correlations play a role in determining how the increments will be spread over the different state variables and throughout the vertical. Because background errors vary both spatially and temporally, they are difficult to accurately estimate.

With a more simple observable that is a function of only type of state variable (e.g. radiosonde temperature measurements), a good analysis can be achieved if the ratio of the background error to the observation error is correctly specified. A scalar weight can be defined for a given observation based on this ratio or vice versa. Therefore, it is not necessary to estimate the correct absolute magnitudes of the both the observation and background errors. However, with satellite radiances that are sensitive to both temperature and humidity, the situation has an added level of complexity. The concept of a single scalar weight cannot be used. The ratio of the temperature and humidity errors projected onto brightness temperature space and its relationship to observation errors becomes important.

This problem, of course, applies to all sounders that have sensitivity to both temperature and humidity (as well as other state variables). These include HIRS, MSU, and AMSU-A, all of which have <20 sounding channels. AIRS has a large number of relatively low noise channels with many in the H_2O band that have narrow weighting functions and are frequently unaffected by low clouds. Therefore, it is likely that the problem of correctly partitioning the increments is amplified with AIRS as compared with the other sounders.

We obtained our best result by simply omitting H_2O band channels from the analysis. There may be a more optimal set of channel errors and quality control thresholds that will provide a better use of these channels. These parameters may be determined experimentally, but the computational cost to do so can be relatively high.

To gain further insight on the sensitivity to the background error specification, we examine examples of the partitioning between temperature and humidity background errors for selected AIRS channels. Background errors are projected to brightness temperature space using HBH^T, as in Andersson *et al*. (2000), where H is the AIRS T_B observation operator Jacobian with respect to state variables x ($\partial T_B/\partial x$) and B is the background error covariance. Examination of HBH^T in conjunction with O-B may help to identify shortcomings in the specification of the matrix B. However, this is beyond the scope of the current work.

Here, we have used background errors and Jacobians from the 1D variational (1DVAR) retrieval system of Joiner and Rokke (2000) linearized about the state shown in Figure 11. The AIRS radiative transfer algorithm of Strow *et al*. (2003) is used for all calculations. The background error standard deviations for temperature and humidity (up to 10 hPa) are given in Table 4. The 1DVAR system qualitatively reproduces the structure of the increments as well as the effects of channel selection shown in Figure 12.

Figure 14 shows how the background temperature and humidity errors are partitioned in terms of AIRS T_B. The background humidity errors are somewhat larger than the temperature errors in the H_2O band. Outside the H_2O band, the background humidity errors are negligible for all but a few channels in the long-wave window. The projected temperature errors can be somewhat larger in the H_2O band channels as compared with similarly peaking channels in the CO_2 bands. This clearly delineates the large sensitivity of the H_2O band channels to temperature as well as humidity and to the specification of background errors.

7. Conclusions and Future Work

We have achieved a significant positive impact on the accuracy of weather forecasts up to five days in both hemispheres by assimilating AIRS and AMSU-A data from the EOS Aqua satellite. The best results were obtained using a set of 156 channels that did not include any from the H_2O band. We find that the assigned channel errors and the different methods of spatial subsetting for AIRS both play a significant role in determining the amount of data that is accepted into our fvSSI DAS. However, we also find that ingesting more AIRS radiances in the DAS does not always translate into improved forecasts. For example, the warmest FOV spatial subsetting yielded improvement in terms of data coverage in partially cloudy conditions. However, although there are indications of a slight improvement with the warmest FOV subsetting in the southern hemisphere, we did not achieve a statistically robust increase in forecast skill.

We find that channels in the H_2O band can have a significant impact on temperature analyses. Although these channels in AIRS-type instruments have been shown in simulations to provide useful information for temperature sounding, the simulations also assume that background and observation errors are known, unbiased, and Gaussian. In reality, these assumptions, especially knowledge of the errors, are likely to be inaccurate. Without a good estimate of the background errors, including their variation in both time and space, assimilation systems cannot fully exploit information from this band. In addition, use of these channels can produce a negative result as we

Published in 2007 by John Wiley & Sons, Ltd.

DOI: 10.1002/qj

Table IV. Background error standard deviations for temperature, σ(T) (K), and natural logarithm of the H_2O mixing ratio $\sigma(H_2O)$ at pressures p (hPa) used in 1DVAR.

p	1000	850	700	500	400	300	250	200	150	100	70	50	30	10
σ(T)	1.9	1.9	1.7	1.7	1.7	1.7	1.9	1.9	1.7	1.6	1.6	1.7	2.5	3
$\sigma(H_20)$	0.2	0.3	0.5	0.5	0.6	0.6	0.7	0.7	0.7	0.7	0.7	0.7	0.7	0.7

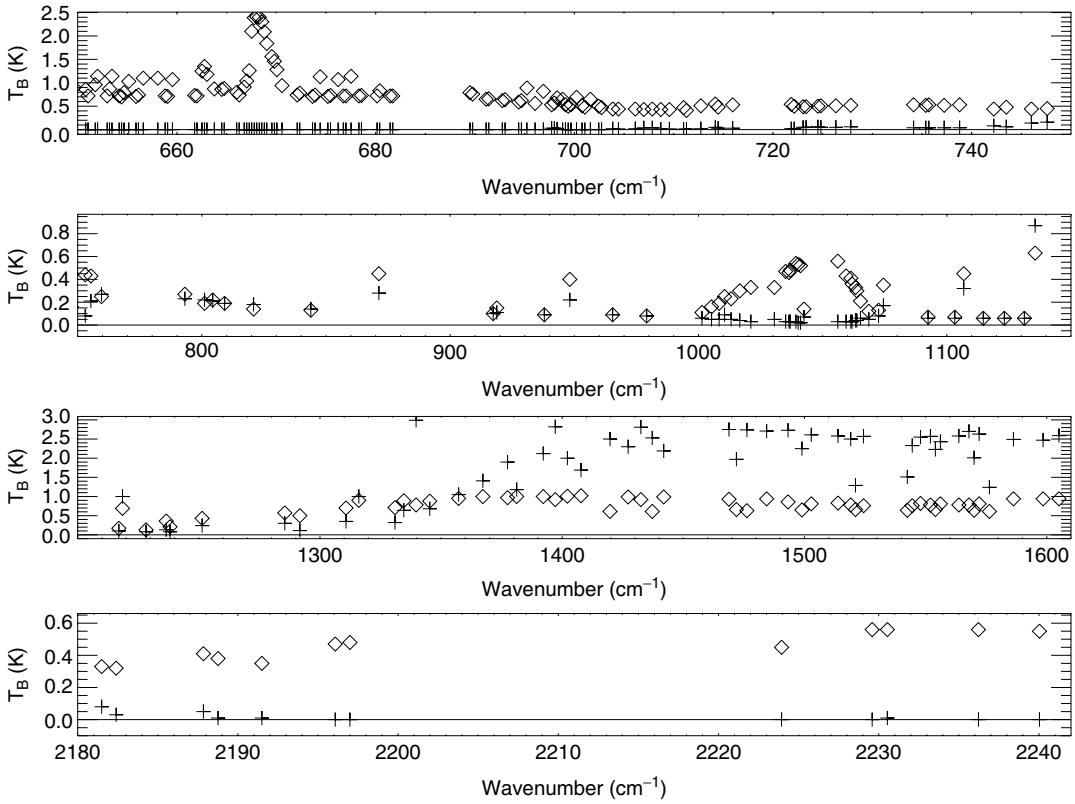

Figure 14. Background errors projected onto AIRS brightness temperatures: ◊: background temperature errors; +: background humidity errors; Solid line: zero line for reference.

have seen here. Our results suggest that one area to target for maximizing the impact of AIRS data is the specification of background errors and in particular the ratio between temperature and humidity errors.

Finally, we do not account for any spectral or spatial correlation in the observation errors. It is likely that forward model errors and/or biases in the observations would produce such correlations. Inclusion of such correlations can change the structure of increments in a data assimilation system.

We caution that the results obtained here may or may not translate to other data assimilation systems. Our experiments are conducted in one season and over a limited time period. It will be interesting to see whether similar results are achieved with other data assimilation systems and for other time periods.

In our experiments, the assigned channel errors affect both the weights those channels receive in the analysis and quality control decisions. In the future, we plan to explore decoupling the background check thresholds from the assigned errors. More sophisticated schemes for spatial subsetting and cloud detection are also being investigated.

Acknowledgements

The authors thank the AIRS science team, particularly M. Chahine and H. H. Aumann for their continued support and enthusiasm, M. Goldberg and W. Wolf for providing timely EOS Aqua AIRS and AMSU-A data, and R. Todling for assistance with the DAS. We also thank two anonymous reviewers and E. Andersson for valuable comments that improved the manuscript. This work was supported by National Aeronautics and Space Administration (NASA) through the Joint Center for Satellite Data Assimilation (JCSDA) and the Modeling, Analysis, and Prediction (MAP) program managed by D. Anderson and T. Lee.

References

Andersson E, Fisher M, Munro R, McNally DA. 2000. Diagnosis of background errors for radiances and other observable quantities in

a variational data assimilation scheme, and the explanation scheme, and the explanation of a case of poor convergence. *Quart. J. Roy. Meteor. Soc.* **126**: 1455–1472.

Aumann HH, Chahine MT, Gautier C, Goldberg MD, Kalnay E, McMillin LM, Revercomb H, Rosenkrantz PW, Smith WL, Staelin DH, Strow LL, Susskind J. 2003. AIRS/AMSU/HSB on the Aqua Mission: Design, science objectives, data products, and processing systems. *IEEE Trans. Geosci. Rem. Sens.* **41**: 253–264.

Chahine MT. 2006. AIRS Improving weather forecasting and providing new data on greenhouse gases. *Bull. Amer. Meteorol. Soc.* **87**: 911–926.

Chen M, Joiner J, Rood RB. 1999. Assimilating TOVS Humidity into the GEOS-2 Data Assimilation System. *J. Clim.* **12**: 2983–2995.

Derber J, Wu W-S. 1998. The use of cloud-cleared radiances in the NCEP SSI analysis system. *Mon. Wea. Rev.* **126**: 2287–2299.

Fourrie N, Rabier F. 2004. Cloud characteristics and channel selection for IASI radiances in meteorologically sensitive areas. *Quart. J. Roy. Meteor. Soc.* **130**: 1839–1856.

Goldberg MD, Qu Y, McMillin LM, Wolf W, Zhou L, Divakarla M. 2003. AIRS Near-real-time products and algorithms in support of operational numerical weather prediction. *IEEE Trans. Geosci. Rem. Sens.* **41**: 379–389.

Joiner J, Rokke L. 2000. Variational cloud clearing with TOVS data. *Quart. J. Roy. Meteor. Soc.* **126**: 725–748.

Joiner J, Poli P, Frank D, Liu HH. 2004. Detection of cloud-affected AIRS channels using an adjacent-pixel approach. *Quart. J. Roy. Meteor. Soc.* **130**: 1469–1487.

Kiehl JT, Hack JJ, Bonan GB, Boville BA, Briegleb BP, Williamson DL, Rasch PJ. 1996. Description of the NCAR Community Climate Model (CCM3). *NCAR Technical Note*, NCAR/TN-420+STR, Boulder, CO, 152 pp.

King MD, Menzel WP, Kaufman YJ, Tanré D, Gao BC, Platnick S, Ackerman SA, Remer LA, Pincus R, Hubanks PA. 2003. Cloud and aerosol properties, precipitable water, and profiles of temperature and water vapor from MODIS. *IEEE Trans. Geosci. Rem. Sens.* **41**: 442–458.

Kleespies TJ, van Delst P, McMillin LM, Derber J. 2004. Atmospheric Transmittance of an Absorbing Gas. 6. OPTRAN status report and introduction to the NESDIS/NCEP community radiative transfer model. *Appl. Opt.* **43**: 3103–3109.

Le Marshall J, Jung J, Derber J, Treadon R, Lord SJ, Goldberg M, Wolf W, Liu HC, Joiner J, Woollen J, Todling R, van Delst P, Tahara Y. 2006. Improving global analysis and forecasting with AIRS. *Bull. Amer. Meteorol. Soc.* **87**: 891–894.

Lin S-J. 2004. A "vertically Lagrangian" finite-volume dynamical core for global models. *Mon. Wea. Rev.* **132**: 2293–2307.

Lin S-J, Atlas RM, Yeh KS. 2004. Global weather prediction and high-end computer NASA. *Comp. Sci. Eng.* **6**: 29–35.

McNally AP. 2002. A note on the occurrence of cloud in meteorologically sensitive areas and the implications for advanced infrared sounders. *Quart. J. Roy. Meteor. Soc.* **128**: 2551–2556.

McNally AP, Derber JC, Wu WS, Katz BB. 2000. The use of TOVS level-1B radiances in the NCEP SSI analysis system. *Quart. J. Roy. Meteor. Soc.* **126**: 689–724.

McNally AP, Watts PD, Smith JA, Engelen R, Kelly GA, Thépaut JN, Matricardi M. 2006. The assimilation of AIRS radiance data at ECMWF. *Quart. J. Roy. Meteor. Soc.* in press.

Menzel P, Strabala K. 1997. Cloud top properties and cloud phase algorithm theoretical basis document, NASA document ATBD-MOD-04, Greenbelt, MD, USA, http://modis-atmos.gsfc.nasa.gov.

Parrish DF, Derber JC. 1992. The National-Meteorological-Centers Spectral Statistical-Interpolation analysis system. *Mon. Wea. Rev.* **120**: 1747–1763.

Rabier F, Fourrié N, Chafai D, Prunet P. 2002. Channel selection methods for Infrared Atmospheric Sounding Interferometer radiances. *Quart. J. Roy. Meteor. Soc.* **128**: 1011–1027.

Strow LL, Hannon SE, De Souza-Machado S, Motteler H, Tobin D. 2003. An overview of the AIRS radiative transfer model. *IEEE Trans. Geosci. Rem. Sens.* **41**: 303–313.

Strow LL, Hannon SE, De Souza-Machado S, Motteler H, Tobin D. 2006. Validation of the AIRS radiative transfer algorithm. *J. Geophys. Res.* **111**: D09S06, doi:10.1029/2005JD006146.